Analytical Modeling of Effects of Wires on Solid Motor Ballistics

Merrill K. King*
Atlantic Research Corporation, Gainesville, Virginia 22065

Metallic wires have been employed in numerous end-burning solid-propellant rocket motors to provide burning-rate amplifications required for certain applications. These wires provide such amplification by locally augmenting heat feedback from propellant combustion products to unburned solid material, with resultant development of cones (and consequent increase in surface area). A model of this process has been developed and tested against an extensive systematic strand-rate data base, with excellent agreement between predicted and measured effects of wire type, wire diameter, and pressure on burning rates. This model is capable of treating unsteady-state phenomena and effects of gaps between wire and propellant, possibly caused by partial wire unbonds from surrounding propellant. The model has been coupled with a chamber ballistic analysis and a geometrical analysis as regards cone shape development to permit prediction of pressure-time histories in wired motors, with gap effects included. A description of the model, discussion of its calibration against the existing wired strand data base, and discussion of effects of various gap distributions on strand burning rates and motor pressure are presented. The model offers a possible explanation for anomalous effects sometimes observed in testing of high L/D (length/diameter) wired motors at low temperature subsequent to temperature cycling.

Nomenclature

$A_{s,\text{total}}$ = total propellant surface area (cone plus flat)
A_t = throat area
C_D = propellant product discharge coefficient
$C_{p,\text{wire}}$ = wire specific heat
$C_{p,\text{prod}}$ = propellant product specific heat
D_{wire} = wire diameter
h_{contact} = heat-transfer coefficient between wire and propellant
k_{prop} = thermal conductivity of propellant
M = product molecular weight
$\dot{m}_{\text{in}}$ = mass generation rate of propellant products
$\dot{m}_{\text{out}}$ = mass flow rate out of motor
P = motor pressure $[f(t)]$
R = universal gas law constant
q'' = heat flux into wire from gas or propellant $[f(t,z)]$
r = radius (Fig. 1)
r_{wire} = wire radius
r'_b = burning rate
r'_{298} = burning rate at 298 K
r'_{matrix} = matrix (unwired propellant) burning rate
r'_{wire} = burning rate of propellant along wire
t = time
T = temperature
T_{gas} = product gas temperature
T_{auto} = propellant autoignition temperature
T_{prop} = local temperature in propellant $[f(t,z,r)]$
$T_{\text{prop,interface}}$ = propellant temperature at wire interface $[f(t,z)]$
T_{wire} = wire temperature $[f(t,z)]$
T_{bulk} = propellant bulk (conditioning) temperature
$\tilde{T}$ = temperature relative to propellant conditioning temperature $(T - T_{\text{bulk}})$
$\tilde{T}_{\text{prop,interface}}$ = $T_{\text{prop,interface}} - T_{\text{bulk}}$
U_{wire} = velocity of product gases immediately adjacent to wire
u = average axial velocity of gases in cone
V_c = free volume of motor chamber $[f(t)]$
V_{surface} = velocity of gases leaving propellant surface (normal to surface)
z = axial direction (Fig. 1)
α_{prop} = propellant thermal diffusivity
β = constant in Eq. (10)
δ = penetration thickness of thermal wave associated with heat transfer from wire $[f(t,z)]$
Δtj = jth time increment
η = nondimensional thermal penetration thickness $[f(t,z)]$
θ = cone angle (Fig. 1)
μ_{gas} = viscosity of product gases
ρ_{gas} = gas density
ρ_{prop} = propellant density
ρ_{wire} = wire density
σ_p = temperature sensitivity of matrix propellant burning rate

Background

SOLID propellants are generally burned in rocket motors in one of two basic configurations, either in the form of an end-burning grain or as a centrally perforated grain. In the end-burner (cigarette-burner) mode, a solid cylinder of propellant is ignited on one end face and burns back along the cylinder parallel to the centerline. In the centrally perforated mode, the propellant cylinder contains a port along the centerline (which may be a simple circular port or may have a much more complex shape such as a star or a wagon wheel) with burning being initiated on the inside of this port, followed by burnback through the cylinder radially to the motor wall. As might be expected, for typical tactical motor length/diameter (L/D) ratios, the end-burning configuration tends to lead to relatively high action times, whereas the centrally perforated configurations yield much shorter times. Because of limited variability of propellant burn rate via formulation adjustment (particularly in the presence of other design constraints), the motor designer sometimes finds himself in a situation where the action times achievable with an end burner are unacceptably long, whereas those achievable with a centrally perforated grain are unacceptably short (within given constraints on motor geometry) for the mission. (In addition, end-burning configurations lead to higher mass fractions, often of consid-

Received June 5, 1989; revision received Feb. 5, 1990.

*Chief Combustion Scientist, Propellant Technology. Associate Fellow AIAA.

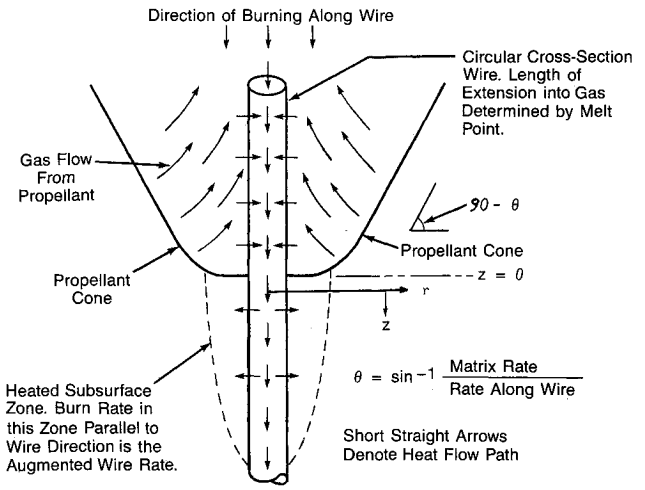

Fig. 1 Schematic of wired propellant combustion.

erable importance, a factor driving the designer to prefer their use.) One way around the problem of excessively long action times for end burners is to embed metallic wires in the propellant, parallel to the motor centerline, to increase effective burning rate.

These embedded metallic wires lead to amplification of the mass burning rate by providing augmented heat feedback from the product gases to the propellant immediately adjacent to the wires, thus resulting in local burn-rate increases in the direction along the wire with consequent formation of cones in the propellant with half-angles equal to the arcsine of the base propellant burn rate divided by burn rate along the wires. The propellant not immediately adjacent to the wire of course burns at its normal rate perpendicular to the cone surface, but because of the increased surface area associated with the cone, the mass generation rate and "effective" burn rate are increased (see Fig. 1). An offshoot of this approach to burn-rate enhancement is the use of chopped metallic fibers (oriented or unoriented) in formulations. (In the oriented-fiber approach, advanced casting technology is applied to cause the fibers to orient themselves preferentially parallel to the direction of burning.)

Rumbel and co-workers[1-3] pioneered the use of embedded metallic wires to enhance solid-propellant burning rates in the mid-1950s, first applying this technology to extrudable polyvinyl-chloride-based composite propellants (designated Arcites). In the course of these early studies, these investigators developed an extensive data base for two formulations, Arcite 155 and 322 (similar formulations differing only in ammonium perchlorate particle size and thus matrix burn rate vs pressure characteristics), utilizing wired strands of propellant burned in a pressurized bomb. This data base encompassed a wide range of pressures, wire diameters, and wire materials (silver, aluminum, copper, tungsten, platinum, and molybdenum). It was found that the burning-rate enhancement was for the most part proportional to the wire thermal diffusivity, with the wire melting temperature having a secondary influence (higher melting point leading to higher rate). For very small diameter wires, burn-rate enhancement was found to increase with increasing wire diameter, up to a diameter of about 5 mil (0.0127 cm), with subsequent decrease in enhancement for further increases in wire diameter.

Subsequently, considerable additional (although not nearly as systematic) data on the effects of wires on burning rates of other composite propellants, notably polybutadiene-based systems, have been amassed at this author's company. In general, however, these studies have been limited to one type of wire and one or, at most, two sizes, with minor formulation adjustments being made in search of a specific wired rate for a specific application. In 1982, Kubota and co-workers[4] published a paper summarizing an experimental study of effects of embedded metal wires on the burning of a series of double-base propellants; wire materials used in this study included silver, tungsten, and nickel, with silver being studied most extensively. (This paper did not include enough information regarding the propellant characteristics to permit comparison of data with predictions by the model developed in the current study.) The wire sizes utilized were all well in excess of 5-mil diameter; augmentation ratios were found to decrease with increasing wire diameter, consistent with the results of Rumbel et al.[1] in this regime. In addition, augmentation ratio was seen to increase with increasing wire thermal diffusivity, again consistent with previous observations.

As part of the early studies by Rumbel and co-workers,[2,3] a simplified heuristic model was developed to qualitatively explain the observed trends regarding effects of wire diameter and type on burning-rate enhancement. This description did qualitatively describe the observations, but required artificial adjustments of parameters not calculated from first principles to actually fit the data. In addition, this model was strictly a steady-state one, incapable of treating transient effects, such as startup or encountering of contact resistances associated with local wire unbonds from the surrounding propellant.

In 1967, Caveny and Glick[5] published a paper describing the effects of embedded metal fibers (actually flat ribbons with a high ratio of one surface dimension to the other, leading to treatment of conduction of heat from the wire into the propellant as a one-dimensional process at each axial location along the wire) on the burning rate of solid propellants. In this analysis, they assumed that the burn rate along the wire is simply the rate at which the point along the wire at which the temperature is equal to some arbitrarily assigned "ignition temperature" propagates along the wire. (This is not to imply that the analysis is simple—it is not.) In addition, no consideration was given to the possibility of a "contact resistance" between the wire and the propellant, a likely result of wire/propellant unbonds that may well occur, for example, as a result of temperature cycling. This model is capable of treating transient effects, being mainly aimed at analysis of the effects of short-chopped metallic fibers on burning rate.

Rybanin and Stesik[6] also analyzed the effects of flat heat-conducting elements on combustion of solid propellants, using an asymptotic solution approach; their analysis is limited to steady-state behavior. More recently, Gossant and co-workers[7] developed a simplified analysis of the effects of circular metal wires on propellant burning rate. Unfortunately, this model encompasses several simplifications that are strongly at odds with experimental observations, the most notable of which are an assumption that the wire does not project above the propellant surface into the gas and a second assumption that the temperature of the wire at the propellant surface is the melting temperature of the wire. With respect to the first assumption, movies of the burning of wired strands have shown that there is significant protrusion of the wires above the propellant surface; the second assumption comes to grief regarding the use of wires with high melting temperatures (e.g., tungsten) which would result in absurdly high propellant temperatures near the propellant-wire-surface interface.

Model Development

A major portion of this section will be devoted to development of the analysis of the effect of a wire on the burning of a propellant strand at constant pressure (with or without gaps between the wire and surrounding propellant). Extension to treatment of motor behavior (with pressure variations coupled in) was relatively straightforward (at least conceptually) and will be described briefly at the end of this section. Circular cross-sectional wires were assumed in this analysis since they are by far the most commonly used in practice. A transient analysis, with an initially flat surface ($\theta = 90$ deg in Fig. 1) and a specified initial projection distance of the wire above the propellant surface, was developed, utilizing the following general strategy.

First, the known product gas temperature and the initial temperature distribution in the wire (to date, the analysis is performed assuming the initial temperature throughout the wire to be equal to the propellant conditioning temperature) are used with a gas-phase heat-transfer analysis (described further in a later section) to calculate the heat flux into the wire at each axial location along the part of the wire extending into the gas. This flux distribution is assumed to remain constant through one time step, which is calculated as the quotient of the user-input axial node spacing divided by the current burn rate along the wire (equal to the matrix rate for the first time step).

A transient analysis of the heat transfer along the wire and into the propellant (again described further in a later section) is then carried out for this first time step, yielding a resultant axial and radial distribution of temperature in the propellant at the end of the time step. The first axial increment of the propellant (increment closest to the surface) is dropped at this point, and the radial temperature distribution at the next node is used to calculate a mean temperature at the "new surface" across a radial thickness equal to three characteristic matrix thermal profile thicknesses (three times propellant diffusivity divided by matrix burn rate). This mean temperature is then used with an expression relating burn rate to temperature (based on the matrix burn-rate temperature sensitivity and autoignition temperature as described later) to calculate a new regression rate value along the wire. This rate is then used in combination with the matrix rate to calculate a new cone angle [θ = arcsine (matrix rate/wire rate)]. The distribution of heat flux into the wire for the next time step is then calculated using the new temperature distribution in the exposed part of the wire and the new cone angle; a new time step is calculated as the quotient of the axial node spacing and the new burning rate along the wire, and the transient heat-transfer analysis in the wire and propellant is restarted and run for this new time increment. A new surface temperature radial distribution is thus defined as that at the next axial node at the end of this time increment; a new mean surface temperature and burning rate along the wire are calculated, and the next calculation loop is started.

Major Assumptions/Approximations

At any given time step through the analysis, the geometry in the vicinity of the wire will have the generic shape of Fig. 1 (with, as mentioned, time zero representing a limiting case where $\theta = 90$ deg and the cone walls are horizontal). This figure is instructive in listing the major assumptions/approximations associated with the analysis:

1) Heat conduction in the propellant parallel to the wire (axial conduction) is neglected.

2) The wire itself is assumed to be thermally thin (no radial temperature gradients in the wire).

3) Gas-phase reaction contributions to the heat balance in the near-wire region are neglected.

4) Radiative heat transport between the wire and surrounding flow is neglected. (Note that this is not the same as neglecting radiative heat feedback to the propellant surface in regions not directly affected by the wire—any contribution in this area is lumped into the empirically input matrix burning rate vs pressure characteristics.) An order-of-magnitude analysis indicates that for a typical wire diameter of 5 mil (0.0125 cm) with a mass flux along the wire of approximately 5 g/cm^2/s, the conductive/convective heat-transfer coefficient between the wire and surrounding flow will be about 0.1 cal/cm^2/s/K, which with a typical temperature difference of approximately 2000 K leads to a heat flux into the wire of about 200 cal/cm^2/s. With an emissivity-absorptivity product of unity, radiative transport, for a gas temperature of 2500 K, will lead to a flux of about 50 cal/cm^2/s, only one-fourth of the conductive/convective flux. Moreover, for more realistic values of the emissivity-absorptivity product of 0.1 or less[8,9] (even for highly metalized propellants, which are not being treated in this study to date), radiative transport contributions will be less than 3% of the conductive/convective contributions.

5) All propellant thermal properties are constant (temperature independent) and isotropic.

6) All wire thermal properties are constant (temperature independent).

7) All wire nodes that reach the melting temperature of the material are assumed to disappear (break off).

8) It is assumed that a unique relationship exists between the burn rate along the wire and a mean temperature (calculated over three matrix thermal profile thicknesses around the wire) for any given formulation.

The last assumption requires further discussion. It is considered that the heating of the propellant adjacent to the wire is equivalent to local raising of the conditioning temperature of the propellant. Thus, for moderate values of "superheat," it is assumed that the matrix propellant burn-rate temperature sensitivity (σ_p) can be used to calculate the augmented rate. However, available temperature-sensitivity data in general are only good up to about 50 deg (Kelvin) of superheat. Accordingly, it was decided to use the autoignition temperature of the propellant as an additional data point, with burn rate set equal to infinity at this temperature. It is assumed that the relationship between burning rate and "effective conditioning temperature" can be expressed in the form:

$$\frac{1}{r_b'} = k_1 + k_2 T + k_3 T^2 \tag{1}$$

with the burn rate at 298 K, the temperature sensitivity over a 50 K range, and the autoignition temperature being used to calculate k_1, k_2, and k_3 for a given formulation from

$$\frac{1}{r_{298}'} = k_1 + 298k_2 + (298)^2 k_3 \tag{2a}$$

$$\frac{1}{r_{298}' \exp(50\sigma_p)} = k_1 + 348k_2 + (348)^2 k_3 \tag{2b}$$

$$0 = k_1 + T_{\text{auto}} k_2 + (T_{\text{auto}})^2 k_3 \tag{2c}$$

Next, one is faced with the question of defining an appropriate temperature for use in Eq. (1) for calculating the burning rate along the wire. One might consider using the surface temperature at the wire-propellant interface, but it seems apparent that this is not really appropriate since it represents the temperature of only an infinitesimal amount of propellant. [In addition, it can be shown that use of such a temperature will result in the predicted rate rising monotonically with decreasing wire diameter all the way to a wire diameter of zero, a result in conflict with observation (and with common sense).] It appears logical that a mean temperature over a thickness of propellant proportional to the characteristic matrix thermal-profile thickness is more appropriate—a thickness equal to three times the propellant diffusivity divided by the matrix rate (equivalent to 95% of the total matrix thermal profile) was chosen as appropriate for the averaging process, giving

$$\bar{T} = \frac{\int_{r_{\text{wire}}}^{r_{\text{wire}} + 3\alpha_{\text{prop}}/r_{\text{matrix}}} rT\, dr}{\int_{r_{\text{wire}}}^{r_{\text{wire}} + 3\alpha_{\text{prop}}/r_{\text{matrix}}} r\, dr} \tag{3}$$

Analysis of Heat Transfer into Wire

An approximate analysis of the gas flowfield in the cone surrounding the wire (Fig. 1) indicates that the velocity component parallel to the wire immediately adjacent to it is proportional to the bulk (average) axial velocity in the cone, with the proportionality constant depending on the cone angle,

varying from unity for a flat surface ($\theta = 90$ deg) to approximately 2.0 for cone angles less than or equal to 45 deg. In addition, the average axial velocity in the cone is related to the gas velocity leaving the cone surfaces by

$$\bar{u} = \frac{V_{\text{surface}}}{\sin\theta} \tag{4}$$

With substitution of $\sin\theta = r'_{\text{matrix}}/r'_{\text{wire}}$ and $\rho_{\text{propellant}}\, r'_{\text{matrix}} = \rho_{\text{gas}}\, V_{\text{surface}}$, the velocity adjacent to the wire can thus be expressed as

$$U_{\text{wire}} = \frac{KV_{\text{surface}} r'_{\text{wire}}}{r'_{\text{matrix}}} = \frac{K\rho_{\text{propellant}}}{\rho_{\text{gas}}}\, r'_{\text{wire}} \tag{5}$$

where K is a function of the cone angle ranging from 1.0 to 2.0. (An empirical fit to the results of the flow analysis is included in the code for calculation of K for any given cone angle.)

The velocity adjacent to the wire is used in calculation of a friction factor and, using Reynolds analogy, a heat-transfer coefficient for heat transport from the product gases into the wire. Laminar flow equations are employed for a Reynolds number (based on wire diameter and axial velocity adjacent to the wire) of less than 2000, while a constant friction factor of 0.008 is used for higher Reynolds number values, leading to

Laminar:

$$q'' = \frac{4KC_{p,\text{prod gas}}}{D_{\text{wire}}} (T_{\text{gas}} - T_{\text{wire}}) \tag{6a}$$

Turbulent:

$$q'' = 0.008\rho_{\text{prop}} r'_{\text{wire}} C_{p,\text{prod}} (T_{\text{gas}} - T_{\text{wire}}) \tag{6b}$$

(Slight modification of this analysis to allow for differences between the angle at the tip of the cone and the "average" angle over the entire cone was carried out during extension of the model to treatment of the effects of wires on motor ballistics.)

Transient Thermal Analysis of Wire and Propellant

Rigorous analysis of the transient heat transfer in the propellant and wire would be extremely difficult, even with the simplifying assumptions listed earlier, involving simultaneous treatment of axial derivative terms in the wire, radial derivative terms in the propellant, and time derivatives in both media. Accordingly, following the lead of Caveny and Glick,[5] the author employed an integral method based on the work of Goodman[10] and Lardner and Pohle[11] to reduce the order of the problem by replacing the differential equations describing the radial heat transfer in the propellant with integral equations based on assumption of a fixed form for the shape of the radial temperature distribution in that region. With this approach, expressions relating the radial heat flux into the propellant at any given axial location and time to the current propellant temperature adjacent to the wire at that axial location and the time-integrated value of local flux up to that time can be used to replace rigorous analysis of the propellant region in supplying needed boundary conditions for solution of the partial differential equation (in time and axial coordinate) governing heat transfer in the wire. (It should be noted in passing that the integral analysis is somewhat more difficult to apply in the current cylindrical geometry than in the one-dimensional geometry treated in Caveny's analysis due to the transcendental nature of the integral equations in the cylindrical geometry case.)

Application of an unsteady-state heat balance to the wire results in the following partial differential equation in temperature (function of time and axial location) along the wire:

$$\rho_{\text{wire}} C_{p,\text{wire}} \frac{\partial T_{\text{wire}}}{\partial t} = k_{\text{wire}} \frac{\partial^2 T_{\text{wire}}}{\partial z^2} + \frac{4}{D_{\text{wire}}} q'' \tag{7}$$

where the sign convention for q'' is such that it represents heat flux into the wire at any axial location. (Recall the assumption of a thermally thin wire, which reduces the wire analysis to a one-dimensional transient problem through neglect of radial temperature gradients in the wire itself.) The boundary conditions for the part of the wire projecting into the gas product stream were discussed in the previous section. For the submerged part of the wire, the heat flux into the wire at any axial location may be expressed as

$$q'' = h_{\text{contact}}(T_{\text{prop,interface}} - T_{\text{wire}}) = k_{\text{prop}} \frac{\partial T_{\text{prop}}(r_{\text{wire}}, t)}{\partial r} \tag{8}$$

where q'', $T_{\text{prop,interface}}$, T_{wire}, h_{contact}, and $\partial T_{\text{prop}}/\partial r$ are all functions of axial location (z) and time. The integral method outlined below is used to relate $q''(z,t)$ to $T_{\text{prop,interface}}(z,t)$ at each axial location and time, and Eq. (8) is then used to eliminate $T_{\text{prop,interface}}$ to establish a relationship between $q''(z,t)$ and $T_{\text{wire}}(z,t)$; Eq. (7) can then be solved numerically using an implicit scheme involving solution of a tridiagonal matrix at each time step.

With neglect of axial temperature gradients in the propellant (assumption 1), the governing equation for temperature distribution in the propellant at any axial location is

$$\frac{\partial(rT)}{\partial t} = \alpha_{\text{prop}} \frac{\partial}{\partial r}\left(r \frac{\partial T}{\partial r}\right) \tag{9}$$

Following the method of Lardner and Pohle[11] for the integral method of analysis in cylindrical coordinates, it is assumed that the temperature-profile shape at any given time and axial location may be expressed as

$$\tilde{T} = T - T_{\text{bulk}} = \beta\left(\frac{\delta + r_{\text{wire}} - r}{r_{\text{wire}}}\right)^2 \ell n\left(\frac{r}{r_{\text{wire}} + \delta}\right) \tag{10}$$

where $\delta(z,t)$ is the thermal-wave thickness in the propellant and β is a constant determined by the boundary conditions. These boundary conditions are

$$r = r_{\text{wire}} + \delta \quad : \quad \tilde{T} = 0, \quad \frac{\partial \tilde{T}}{\partial r} = 0 \tag{11a}$$

$$r = r_{\text{wire}} \quad : \quad q'' = k_{\text{prop}} \frac{\partial \tilde{T}}{\partial r} \tag{11b}$$

Application of these boundary conditions, and substitution of $\eta(z,t) = [\delta(z,t) + r_{\text{wire}}]/r_{\text{wire}}$ leads to

$$\tilde{T} = \frac{(q'' r_{\text{wire}}/k_{\text{prop}})(\eta - r/r_{\text{wire}})^2 \ell n(r/r_{\text{wire}}\eta)}{(\eta - 1)(2\ell n\eta + \eta - 1)} \tag{12}$$

which when evaluated at the propellant-wire interface ($r = r_{\text{wire}}$) yields

$$\tilde{T}_{\text{prop,interface}} = \frac{-(q'' r_{\text{wire}}/k_{\text{prop}})(\eta - 1)\ell n\eta}{2\ell n\eta + \eta - 1} \tag{13}$$

Integration of both sides of Eq. (9) over the thermal-wave thickness (r_{wire} to $r_{\text{wire}} + \delta$), followed by substitution of the flux boundary condition at the wire-propellant interface [second part of Eq. (8)] and considerable mathematical manipulation, leads to an expression relating the thermal-profile thickness at a given time, the flux at that time, and the time integral of the flux up to that time (all at a given axial location):

$$-\alpha_{\text{prop}}/r_{\text{wire}}^2 q'' \int_0^t q''\, dt = f(\eta) \tag{14}$$

where

$$f(\eta) = \frac{(72\eta^2 - 96\eta + 36)\ell n\eta + 36\eta^2 - 13\eta^4 - 32\eta + 9}{144(\eta - 1)(2\ell n\eta + \eta - 1)} \quad (15)$$

The heart of the integral analysis lies in breaking the integral of Eq. (14) down to

$$\int_0^t q''\,dt = \int_0^{t-\Delta t_j} q''\,dt + \frac{q''(t-\Delta t_j) + q''(t)}{2}\Delta t_j \quad (16)$$

with the integral on the right-hand side of the equation being updated and stored at each time step.

A brief outline of the procedure for analyzing heat transport in the wire and propellant using the integral method for the propellant follows. For any time step Δt_j, new values of T_{wire} are calculated at each axial node along the wire using one time step of numerical integration of Eq. (7) with the old (previous time step) flux values (lagging solution). New values of propellant temperature at the wire-propellant interface, η (dimensionless thermal wave penetration), and flux are then calculated at each axial location using Eqs. (13-16) along with the first part of Eq. 8 in a trial-and-error-loop calculation. [For cases with very small or no gap between the wire and propellant, the old flux values could be used to calculate the temperatures via Eq. (8), with subsequent solution of Eqs. (13-16) for new flux values, but with gaps of more than a few microns, this simpler procedure was found to break down.] The new values of flux are then used to update the flux-time integrals at each node and are also used as boundary conditions in treatment of the next time step in the integration of Eq. (7) with respect to time.

Treatment of Melting-Wire Effects

Some of the wire materials employed in wired propellant grains have fairly low melting points (e.g., 930 K for aluminum, 1230 K for silver, 1355 K for copper); early calculations with a computer code based on the analysis described in the preceding sections showed that these temperatures would be quickly exceeded at the outer reaches of the exposed wires as the propellant receded back around them. It is postulated that the shear forces associated with the product flow along the wires (out of the cones) will instantaneously remove any wire nodes whose temperature rises above the melting point of the material being used. Accordingly, the code was modified to drop at each time step any wire nodes predicted to rise above the melting temperature during the preceding time increment. In this analysis, the heat of melting is straightforwardly decremented from the heat balance on the wire via modification of the wire-tip boundary condition to include a heat-of-melting term for the mass associated with the dropped nodes.

Extension of Model to Calculation of Motor Ballistics

Extension of the model described above, developed for calculation of the effects of wires on propellant strand rates (fixed pressure) with and without gaps between the wire and the propellant, to treatment of motor ballistics (with time-dependent pressure and matrix rate) involves addition of geometric (cone development) and ballistic analysis steps (along with the slight modification of the analysis of heat transfer from product gases into the wire, alluded to earlier). For simplicity (at least at present), the motor analysis is currently limited to treatment of a cylindrical end-burning grain with a single wire down its center. (Gap width between the wire and surrounding propellant is allowed to vary with distance along the wire for parametric study of the influence of nonconstant gaps on ballistics.) As the propellant burns back along the wire, successive segments of propellant surface with orientations determined by the angle at the tip of the cone at the time of their generation are added to the developing cone. These segments subsequently burn back normal to their orientations at the pressure-dependent matrix burning rate (function of time through dependence of pressure on time). At each successive time point, each segment is moved back normal to its orientation by a distance equal to the product of the instantaneous matrix rate and the time increment, and new intersections of adjacent segments are calculated for definition of a new cone surface profile. (As part of this procedure, segments can of course disappear upon convergence of their normal bisectors—this is treated in the geometrical analysis.) As the intersection of the first segment generated with the remaining initial flat surface (which is of course also receding) moves outward, the motor wall is eventually reached (no more surface normal to the motor axis) and treatment of successive intersections of the cone with the wall is brought into the geometrical analysis.

Definition of the full shape of the cone and the amount of flat surface not yet engulfed (up to the point at which the cone intersects the wall) permits straightforward calculation of total propellant surface area at any given time. This value is then used in a simplified chamber ballistics analysis (in which product temperature variations due to pressurization/depressurization are neglected) to calculate the evolution of motor pressure and free volume with time using Eqs. (17-20):

$$\dot{m}_{in} = \rho_{prop} r'_{matrix} A_{s,total} \quad (17)$$

$$\dot{m}_{out} = C_D A_t P \quad (18)$$

$$V_c \frac{M}{RT_{gas}} \frac{dP}{dt} = \dot{m}_{in} - \dot{m}_{out} \quad (19)$$

$$\frac{dV_c}{dt} = \dot{m}_{in}/\rho_{prop} \quad (20)$$

Comparison of Model Predictions and Data

As indicated earlier, an extensive data base on the effects of wires on propellant burning rates was developed by Rumbel et al.[1] for two polyvinyl-chloride-ammonium perchlorate solid-propellant formulations in the 1950s. In this investigation, in which wired propellant strands were burned in a pressurized bomb, wire type, wire diameter, and pressure were systematically varied independently; thus, this data base provides an excellent test vehicle for the model developed in the current study. In addition, data obtained more recently by Atlantic Research for a polybutadiene-based composite propellant are examined. Compositions for the three formulations studied along with propellant properties needed for model inputs are given in Table 1. As may be seen, the two polyvinyl chloride formulations (Arcites 155 and 322) are nearly identical, differing only in ammonium perchlorate size distribution (and thus matrix burning rate). Data obtained with six different wire materials (silver, copper, tungsten, platinum, aluminum, and

Table 1 Propellant properties of formulations examined

	Arcite 155, 322	Arcadene 426
Nominal composition	74.62 AP 12.44 PVC resin 12.44 dibutyl sebacate 0.50 stabilizer	85.0 AP 12.5 HTPB 12.5 dioctyladipate
Flame temperature, K	2471	2838
Product specific heat, cal/g K	0.43	0.445
Density, g/cm^3	1.645	1.67
Propellant specific heat, cal/g K	0.385	0.375
Propellant thermal conductivity, cal/cm s K	0.00062	0.00071
σ_p, % per K	0.22	0.25
Matrix rates at 1000 psia, cm/s	1.14, 1.27	1.70

Table 2 Wire properties for wire materials used

Material	Thermal conductivity, cal/cm s K	Density, g/cm^3	Specific heat, cal/g K	Thermal diffusivity, cm^2/s	Melt temperature, K	Heat of melting, cal/g
Silver	0.95	10.50	0.068	1.33	1230	26
Copper	0.90	8.92	0.106	0.95	1355	50
Tungsten	0.42	19.35	0.035	0.62	3950	46
Platinum	0.28	21.45	0.035	0.37	2030	24
Aluminum	0.55	2.70	0.290	0.70	930	95
Molybdenum	0.35	10.20	0.070	0.49	3160	73

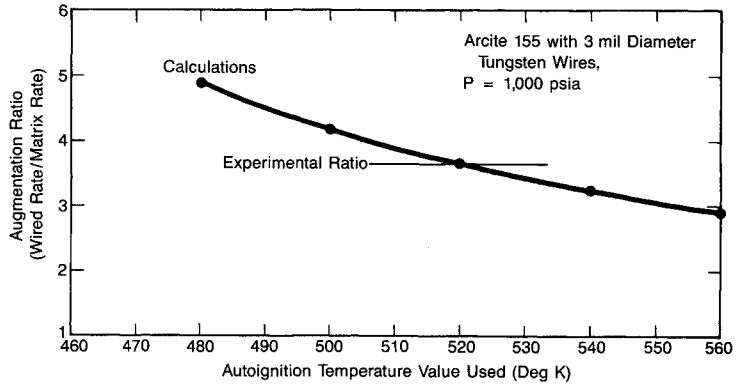

Fig. 2 Sensitivity of calculated wired propellant burning rate to input autoignition temperature.

molybdenum) were compared to model predictions in this study; properties of these materials required as model inputs are tabulated in Table 2.

As mentioned in discussion of the model development, allowance was made in the model for a finite contact resistance (variable with axial distance along the wire via user input) between the wire and propellant to permit simulation of the effects of gaps resulting from wire unbonds (caused in motor situations, for example, by temperature cycling resulting in different expansions/contractions of the propellant and the metallic wires which tend to have large differences in coefficients of thermal expansion). All calculations presented in this section were performed using a negligible contact resistance (very high value of h_{contact}) under the logical assumption that no such unbonds were present with the wired strands. In all cases, the model was run until an asymptotically limiting value of burn rate along the wire was achieved (generally at 0.5–1.0 cm of total regression along the wire).

The one needed propellant property that is not well documented (and, in fact, not even very well defined) is the autoignition temperature, required for evaluation of the constants appearing in the burning rate vs temperature equation [Eq. (1)]. Discussions with various propellant developers indicate that physically realistic values of this parameter probably are bounded by 450 and 600 K (350–620°F). A rough optimization of choice of value for this parameter was carried out by comparison of model predictions with data obtained at 1000 psia with various diameter tungsten wires, resulting in a chosen value for autoignition temperature of 520 K (475°F) for the Arcites. Sensitivity of predicted augmentation ratios (wired rate/matrix rate) to this parameter was examined; results of this sensitivity study for 3-mil-diam tungsten wires in Arcite 155 are presented in Fig. 2. As may be seen, variation of the autoignition temperature value from 480–560 K ($\pm$ 40 K around the selected 520 K value) leads to a variation in augmentation ratio from 4.8–2.9 ($\pm$ 30% around the 3.65 value). Thus, it may be seen that the sensitivity of predicted wired rates to this parameter, while not overwhelming, is certainly not negligible; further information for fitting of the constants in Eq. (1) (for example, temperature sensitivity data out to much higher temperatures than normally examined) would be highly desirable.

In Table 3, predicted 1000 psia burning rates and augmentation ratios are compared with data for Arcite 322 containing 5-mil-diam wires of different materials (silver, copper, tungsten, platinum, and aluminum). In all model runs, the autoignition temperature of the propellant is held at the 520 K value established from the earlier analysis of the tungsten wire data with Arcite 155. As may be seen, the model does a reasonably good job of predicting the effects of the various materials on wired burning rates, although it does overpredict the augmentation ratio by about 17% for silver and 27% for aluminum, while underpredicting the effect of platinum by about 22%. It should be noted that the conductivity value used for aluminum may well be too high. It has been observed that electrical conductivity of aluminum is strongly decreased in the presence of even low levels of impurities, and it is generally found that thermal conductivity tracks well with electrical conductivity. Thus, if there were impurities in the aluminum wire used the thermal conductivity may well have been lower than the value used in the modeling exercise; reduction of this value from 0.55 to 0.45 cal/cm s K would result in excellent agreement between model predictions and data.

In Fig. 3, predicted and experimental wired burning rates for Arcite 155 at 1000 psia are plotted against wire diameter for tungsten, molybdenum, copper, and silver wires. As may be seen, the model predicts the existence of a wire diameter for which the rate is maximized, with the rate rolling off fairly quickly for smaller diameters and more gradually for larger diameters; for the four wire materials studied, the rate-maximizing diameters are predicted to be 3–4 mil. In general, the model predictions agree reasonably well with the data both in terms of general magnitude of the wire-effect and wire-diameter dependency. With tungsten wires, agreement between theory and data is excellent and with molybdenum and copper the degree of agreement is certainly respectable. Even with silver wires the trends appear to be correctly predicted although the magnitude of the wire effect is overpredicted for silver wires as with Arcite 322. On the whole, the model predictions appear to be quite acceptable, particularly considering the lack of adjustable parameters.

A predicted burning rate vs pressure curve for Arcite 155 with 3-mil-diam tungsten wires is plotted along with five data

Table 3 Comparison of predicted and experimental burn rates for Arcite 322 with various 5-mil-diam wires at P = 1000 psia

Wire type	Burn rate cm/s		Augmentation ratio		
	Experimental	Calculated	Experimental	Calculated	
Silver	6.73	7.85	5.30	6.18	17% high
Copper	5.89	5.40	4.63	4.25	8% low
Tungsten	4.62	4.39	3.64	3.46	5% low
Platinum	3.71	2.88	2.92	2.27	22% low
Aluminum	2.95	3.75	2.32	2.95	27% high

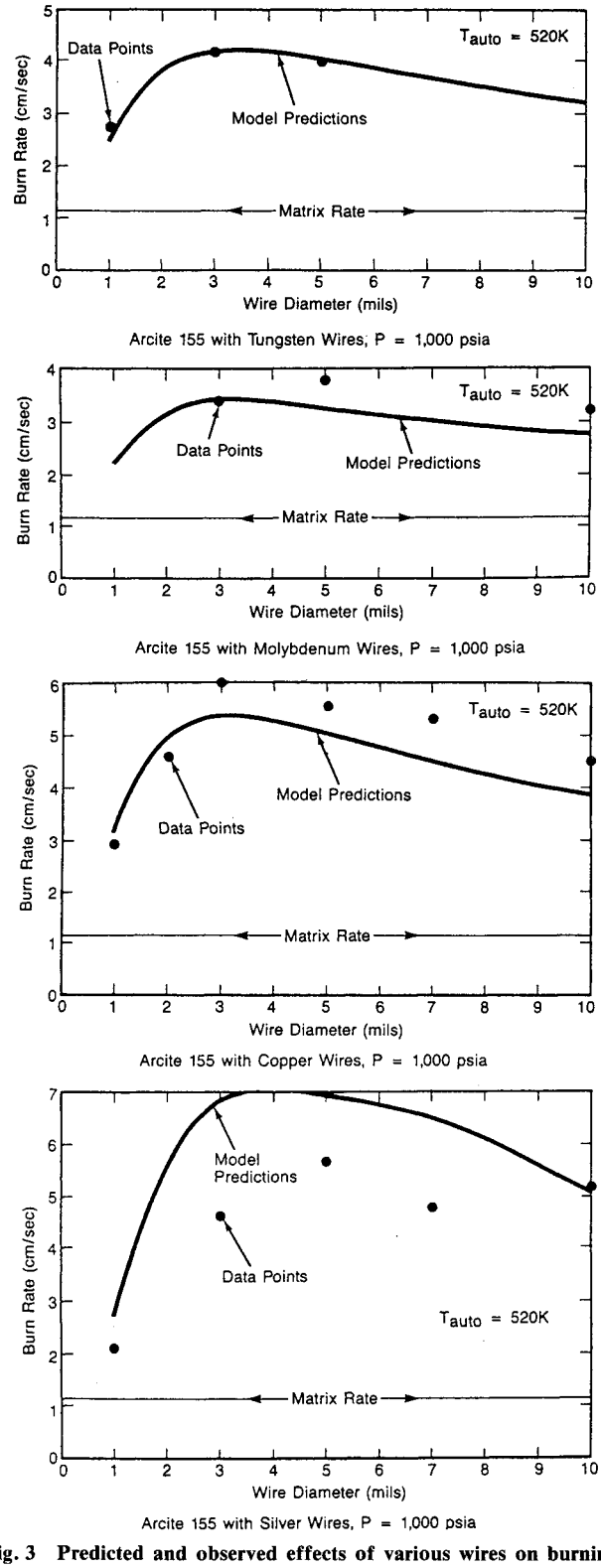

Fig. 3 Predicted and observed effects of various wires on burning rate.

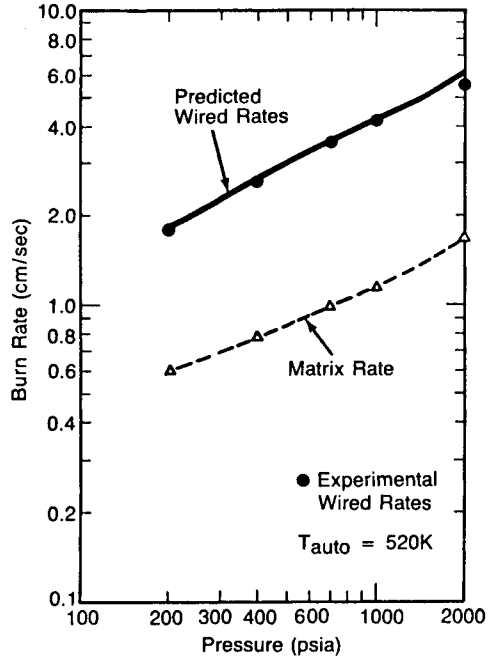

Fig. 4 Arcite 155 with 3-mil-diam tungsten wires.

points in Fig. 4; as may be seen, the degree of agreement is outstanding. In Fig. 5, a similar burning rate vs pressure presentation of data and predictions is made for Arcadene 426 with 10-mil-diam silver wires. Because of major differences in this formulation from the Arcites (Table 1), it is reasonable to expect that the effective autoignition temperature of this propellant might well differ from the 520 K value used for the Arcites. Predicted burning rate vs pressure curves calculated using autoignition temperatures of 550, 600, and 620 K are presented in Fig. 5, along with wired propellant and matrix data. It is observed that reasonably good agreement between theory and data is found with T_{auto} = 600 or 620 K, while use of T_{auto} = 550 K leads to overprediction of augmentation ratio by about 15–20%. It should be recalled, however, that the effect of silver wires was overpredicted for the Arcite formulations. Thus, it might be that the 550-K value would prove to be more reasonable in predictions of Arcadene 426 behavior with other wire materials; unfortunately data for such a comparison have not been found.

Predicted Effects of Gap Width on Wired Strand Rate

Following completion of the calibration of the strand version of the wired burning-rate model with respect to the data base described in the previous section, parametric studies of the effects of gaps between the wire and surrounding propellant on strand burning rate were carried out. Arcadene 426 burning at 200 psi with an embedded 10-mil-diam silver wire was arbitrarily chosen for these studies. An autoignition temperature for this formulation of 560 K, based on the rationale presented in the last section, was used in generation of the results presented here; trends observed were only slightly affected by use of autoignition temperatures over the range presented in Fig. 5. In calculation of the heat-transfer coeffi-

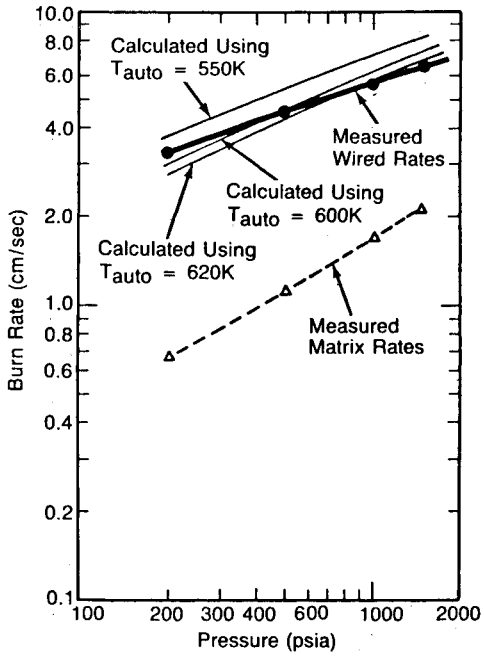

Fig. 5 Arcadene 426 with 10-mil-diam silver wires.

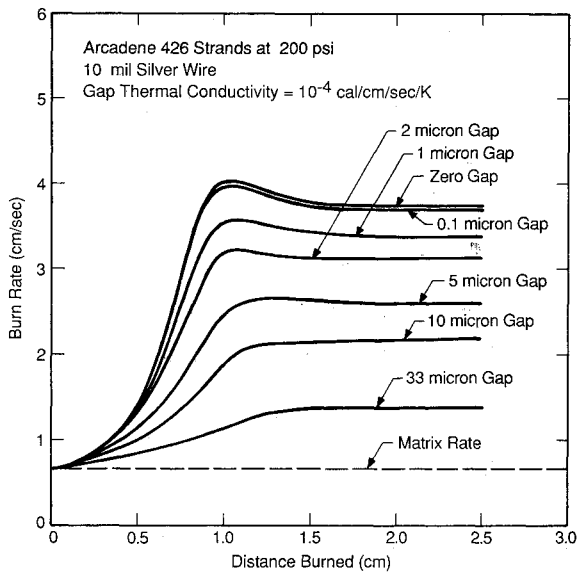

Fig. 6 Effect of gap between wire and propellant on burning rate vs distance burned.

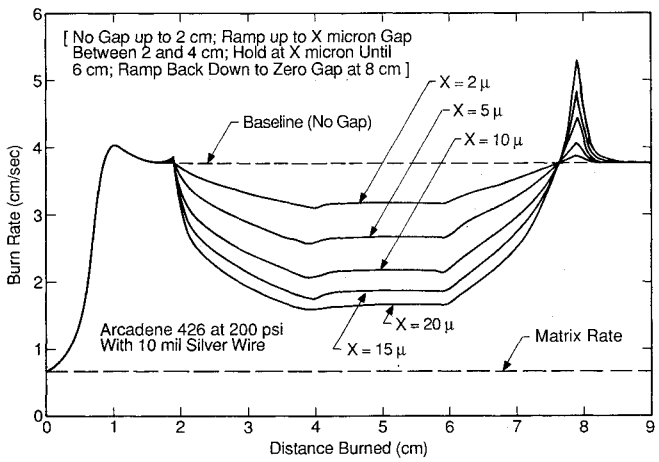

Fig. 7 Effect of ramp changes in gap width on strand burning rate vs distance burned.

cient across the gap [$h_{contact}$ in Eq. (8), the quotient of the thermal conductivity of the gap medium, and the gap width], a value of 0.0001 cal/cm/s/K was used for the thermal conductivity of the gap gases (corresponding to nitrogen at about 400 K), again somewhat arbitrarily. (Obviously, if a different value is chosen, the results presented can be easily adjusted by ratioing gap widths proportionally to the conductivity values.)

In Fig. 6, the effect of the gap size on strand burning rate vs distance burned (again assuming an initially flat surface) is presented. Included for reference are the matrix rate for Arcadene 426 at 200 psi and the predicted burn rate vs distance burned for perfect contact between the wire and the propellant (no gap). As may be seen, the shapes of the curves for the various gap widths are somewhat similar, although the overshoot in burn rate predicted at zero or small gap width (resulting from the finite time required for the quasisteady temperature profile in the wire to be established) does disappear for gap widths in excess of about 5–10 μm (0.2–0.4 mil). As also shown by this figure, the asymptotic strand rate decreases monotonically with increasing gap width, as expected, with the augmentation ratio (wired rate divided by matrix rate) decreasing from about 7 in the case of no gap, to 4 for a 5-μm (0.2 mil) gap to 2 for a 33-μm (1.3 mil) gap.

In Fig. 7, results of examination of the effects of ramp changes in gap size between the wire and propellant, representing regions of opening and closing gaps, are presented. In this scenario, the gap is held at zero for the first 2 cm along the wire, with a ramp up to a designated value over the next 2 cm, followed by a hold at the designated value for the next 2 cm, and finally a ramp back to zero gap width over the next 2 cm. Designated gap-width values examined in this part of the study were 2, 5, 10, 15, and 20 μm. As may be seen, overshoots do occur, particularly during the gap-disappearance phase, but they are not severe. (Similar studies with step changes in gap width indicated severe overshoots under that more severe scenario.) The flat portions of the burning rate vs distance burned curves, appearing over most of the period of constant gap width, agree well with the quasi-steady-state values for the corresponding gap widths presented as the straight-line sections of Fig. 6.

Prediction of Motor Pressure Behavior

Next, the complete model, including treatment of cone shape development and motor chamber ballistics coupled with the analysis of wire heating effects on propagation of the cone tip along the wire, was utilized in a limited study of the effects of wires on motor ballistic behavior, with and without the presence of gaps between wire and propellant. The Arcadene 426 propellant (Table 1) with a single 10-mil-diam silver wire embedded along the motor axis was used for this study; motor parameters chosen are summarized in Table 4. A fairly small motor was used in this study since larger motors generally use more than one wire, a scenario not yet treatable with this model. An initially flat surface (no preconing) was assumed; the chosen motor parameters yield an initial motor pressure (steady-state pressure without the wire) of about 3 atm. It should be noted that the pressure exponent of the chosen propellant is fairly high (0.577) leading to strong magnification of wire effects on motor operating pressure.

First, the effects of various constant gap widths between wire and propellant were examined; results are presented in Fig. 8. As may be seen from this figure, the model predicts considerable (order of 20%) overshoot in pressure above the asymptotic value due to interactions between wire heat up processes and cone development processes. The asymptotic pressure level (right side of the figure) is predicted to decrease strongly with increasing gap width, due to a combination of the strong sensitivity of propagation rate along the wire to gap width (shown earlier) and the relatively high burning-rate pressure exponent.

Finally, the effects of several scenarios as regards gap-width distribution along the wire were examined; results of these

Table 4 Motor parameters for motor pressure-time history cases studied

Arcadene 426 propellant
10-mil-diam silver wire
BR, cm/s = $0.149P^{0.577}$ (P in atmospheres)
Product MW = 24.65
C-Star = 4900 ft/s
Throat area = 0.041 cm^2
Motor ID = 1.5 cm
Initial free volume = 10 cm^3
Equilibrium pressure w/o wire = 2.938 atm
Initially, flat surface (no precone)
One wire

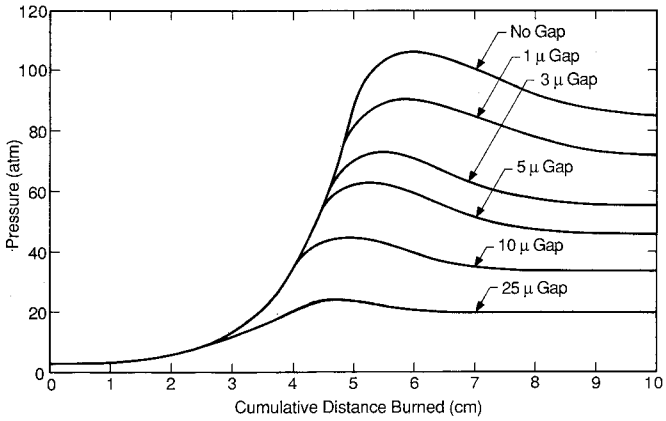

Fig. 8 Baseline motor test case—various gap widths.

studies are presented in Fig. 9. In each part of this figure, the gap width vs distance burned profile is presented at the bottom of the panel, with the resulting predicted pressure being presented at the top of the panel. (The first 8 cm of each case are omitted since the gap width in all cases was zero over this portion of the run, leading to identical results.) In all cases examined, the maximum gap width was 10 μm (0.4 mil).

As may be seen from panel A, a 2-cm ramp up to 10-μm gap width, followed by 2 cm at this gap width, followed by a 2-cm ramp back to zero gap results in a slightly distorted pressure vs time pattern, with a modest undershoot in pressure relative to the 10-μm gap asymptotic value. With a 2-cm ramp-up followed by an immediate 2-cm ramp back to zero gap (panel B), a fairly regular waveform is obtained, with pressure not quite dropping to the asymptotic value of 33 atm associated with a 10-μm gap. Skipping to panel D, where the ramp times are halved, we again see a regular waveform, but the minimum pressure produced in this case is even further above the 10-μm gap asymptotic value.

In panels C and E, the effects of repeated sawtooth ramps corresponding to the single sawtooth patterns of panels B and D are presented; as may be seen, approximately the same pressure minima are predicted, but the pressure does not return to anywhere near the zero-gap asymptotic value during the intermediate returns of gap width to zero, only returning to that value after cessation of the gap-width cycling.

This preliminary study demonstrates that the existence of gaps between the wire and propellant in wired motors can have major impact on motor pressure behavior, with considerable variation of pressure with time and considerable reduction in average operating pressure (and thus mass flow and thrust). Such behavior has indeed been observed in high L/D wired motors that have been temperature cycled and then fired at low-temperature conditions (but not when the motors are temperature cycled and fired at normal ambient or high temperature). It is suspected that the temperature cycling, due to large differences in thermal expansion coefficient of wire and propellant, leads to unbonds between wire and propellant

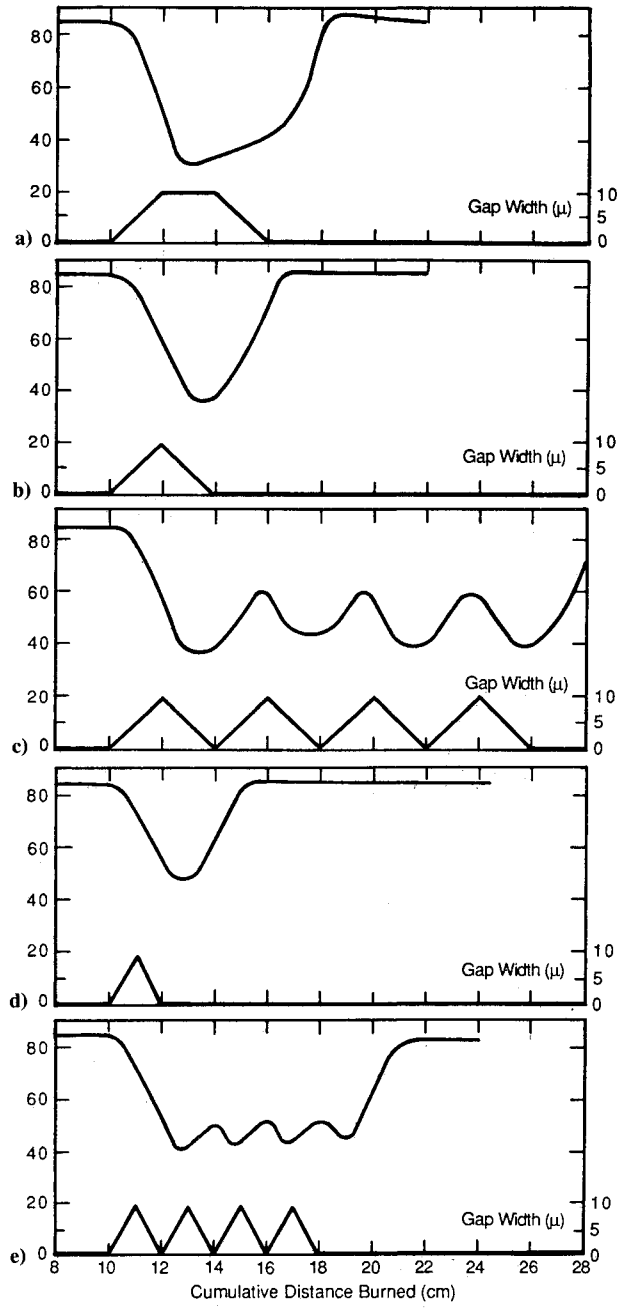

Fig. 9 Pressure (atm) vs cumulative distance burned for various gap-width schedules.

causing sporadic gaps between the wire and the propellant which cannot relax back to zero gap at low-temperature conditions where the propellant is considerably less elastic than at normal ambient or high-temperature conditions.

References

[1]Rumbel, K. E., Cohen, M., Henderson, C. B., and Scurlock, A. C., "A Physical Means of Attaining High Burning Rate in Solid Propellants," Eleventh Army-Navy-Air Force Solid Propellant Meeting, Washington, DC, May 1955, p. 155.

[2]Grover, J. H., Rumbel, K. E., Rice, M. L., Weil, L. L., Sloan, A. W., and Scurlock, A. C., "Research and Development Programs in Fields of Solid Propellants and Interior Ballistics," Supplement to QPR No. 26, Rept. to U.S. Navy Bureau of Ordnance, May 1960.

[3]Friedman, R., Henderson, C. B., and Rumbel, K. E., "Factors Governing Burning Characteristics of Composite Solid Propellant," 1959 JANAF Meeting, Washington, DC.

[4]Kubota, N., Ichida, M., and Fujisawa, T., "Combustion Processes of Propellants with Embedded Metal Wires," *AIAA Journal,*

Vol. 20, Jan. 1982, p. 116.

[5]Caveny, L. H., and Glick, R. L., "Influence of Embedded Metal Fibers on Solid-Propellant Burning Rate," *Journal of Spacecraft and Rockets,* Vol. 4, Jan. 1967, p. 79.

[6]Rybanin, S. S., and Stesik, L. N., "Theory of Combustion of a Condensed Propellant with a Flat Heat-Conducting Element," *Combustion, Explosives, and Shockwaves*, Vol. 10, Feb. 1976, p. 553.

[7]Gossant, B., Godfrey, F., and Robert, P. H., "Theoretical Calculus of Burning-Rate Ratio in Grains with Embedded Metal Wires," AIAA Paper 88-3255, July 1988.

[8]Zennin, A. A., Glaskova, A. P., Leipunskyi, O. I., and Bobolev, V. K., "Effect of Metallic Additives on the Deflagration of Condensed Systems," *Twelfth Symposium (International) on Combustion,* Combustion Inst., Pittsburgh, PA, 1969, p. 27.

[9]Felton, R. F., and Hitchcock, J. E., "An Optical Technique to Measure Radiant Energy Incident on a Burning Solid-Propellant Surface," AIAA Paper 71-469, April 1971.

[10]Goodman, T. R., "Applications of Integral Methods to Transient Nonlinear Heat Transfer," *Advances in Heat Transfer*, Academic Press, New York, 1964, p. 52.

[11]Lardner, T. J., and Pohle, F. V., "Application of the Heat Balance Integral to Problems of Cylindrical Geometry," *Transactions of the ASME Journal of Applied Mechanics*, Vol. 28, No. 2, 1961, p. 310.